Journal of Luminescence 154 (2014) 362–368

Contents lists available at ScienceDirect

Journal of Luminescence

journal homepage: www.elsevier.com/locate/jlumin

Mathematical characterization of continuous wave infrared stimulated luminescence signals (CW-IRSL) from feldspars

V. Pagonis [a,*], Huy Phan [a,b], Rebecca Goodnow [a,b], Sara Rosenfeld [a,b], P. Morthekai [c]

[a] Physics Department, McDaniel College, Westminster, MD 21157, USA
[b] Luminescence Dating Laboratory, CSIR-National Geophysical Research Institute, Hyderabad 500007, India
[c] Birbal Sahni Institute of Palaeobotany, 53 University Road, Lucknow 226007, India

ARTICLE INFO

Article history:
Received 20 January 2014
Received in revised form
28 March 2014
Accepted 5 May 2014
Available online 14 May 2014

Keywords:
Feldspar IRSL curves
Random defect model
Becquerel decay law

ABSTRACT

Continuous-wave infrared stimulated luminescence signals (CW-IRSL) from feldspars have been the subject of many experimental studies, due to their importance in luminescence dating and dosimetry. Accurate mathematical characterization of the shape of these CW-IRSL signals in feldspars is of practical and theoretical importance, especially in connection with "anomalous fading" of luminescence signals in dating studies. These signals are known to decay in a non-exponential manner and their exact mathematical shape as a function of stimulation time is an open research question. At long stimulation times the IRSL decay has been shown experimentally to follow a power law of decay, and previous researchers have attempted to fit the overall shape of these signals empirically using the well known Becquerel function (or compressed hyperbola decay law). This paper investigates the possibility of fitting CW-IRSL curves using either the Becquerel decay law, or a recently developed analytical equation based on localized electronic recombination of donor–acceptor pairs in luminescent materials. It is shown that both mathematical approaches can give excellent fits to experimental CW-IRSL curves, and the precision of the fitting process is studied by analyzing a series of curves measured using a single aliquot of a feldspar sample. Both fitting equations are solutions of differential equations involving numerically similar time dependent recombination probabilities $k(t)$. It is concluded that both fitting equations provide approximately equivalent mathematical descriptions of the CW-IRSL curves in feldspars, and can be used as mathematical representations of the shape of CW-IRSL signals.

1. Introduction

The study of continuous-wave infrared stimulated signals from feldspars (CW-IRSL) is of great importance in luminescence dosimetry and luminescence dating. These signals are known to decay in a non-exponential manner and the exact mathematical shape of these curves is an open research question [1–3]. Accurate mathematical characterization of the shape of these signals in feldspars is also of importance in connection with "anomalous fading" of luminescence signals in dating studies ([4–7]; and references therein). Several studies have suggested that anomalous fading is due to quantum mechanical tunneling from either the ground state or from the excited state of the trap, and that this ground state tunneling process in various materials can be described by power-law decay [4–34].

The well-known Becquerel decay law has been shown to be a very effective tool for the analysis of a variety of luminescence signals. The mathematical properties of this decay law have been presented in detail by Berberan-Santos [26] and Berberan-Santos et al. [27], and in the references therein. Several researchers have suggested that the CW-IRSL signals from feldspars can be analyzed accurately using the Becquerel decay law for luminescence. Bailiff and Poolton [8] studied the charge transfer mechanisms in several feldspar samples and fitted CW-IRSL curves using non-first order kinetics, while Bailiff and Barnett [6] compared the shape of CW-IRSL curves at 290 K and 160 K. Baril [17] showed that the CW-IRSL curves follow a power decay law at long stimulation times and provided an extensive discussion and study of this power-law, as applied to several types of luminescence signals from feldspars. Molodkov et al. [23] reported on kinetics, temperature dependence and number of components for tunneling afterglow in the optically stimulated luminescence of feldspar samples. These authors also found that the fading of the tunneling luminescence follows Becquerel's empirical law.

It is noted that all these previous CW-IRSL studies used the Becquerel law in an empirical fashion, and the reason for the successful fitting of CW-IRSL signals using this law has never been explained adequately.

* Corresponding author. Tel.: +1 410 857 2481; fax: +1 410 386 4624.
E-mail address: vpagonis@mcdaniel.edu (V. Pagonis).

http://dx.doi.org/10.1016/j.jlumin.2014.05.008
0022-2313/

Recently Jain et al. [22] developed a new general kinetic model describing localized electronic recombination of donor–acceptor pairs in luminescent materials. Recombination in this model is assumed to take place via the excited state of the donor, and to take place between nearest-neighbors within a random distribution of centers. These authors found good agreement between two versions of their model, an exact model that evolves in both space and time, and an approximate semi-analytical model evolving only in time. Jain et al. [22] simulated successfully both thermally stimulated luminescence (TL) and optically stimulated luminescence (OSL) phenomena, and demonstrated the power law behavior for simulated OSL signals.

The semi-analytical version of the model by Jain et al. [22] was examined by Kitis and Pagonis [28] who showed that the system of simultaneous differential equations can be approximated to a very good precision by a single differential equation which was solved analytically for four different experimental modes of stimulation: TL, OSL, linearly modulated OSL (LM-OSL) and isothermal TL processes. The analytical equations were tested by successfully fitting typical experimental CW-IRSL signals and TL glow curves from feldspar samples.

The goals of the present paper are:

(a) To investigate the possibility of fitting experimental CW-IRSL curves by using two mathematical approaches, namely the analytical equation derived by Kitis and Pagonis [28] and the well-known Becquerel decay law.
(b) To investigate the range of numerical values, as well as the precision of the fitting parameters extracted from experimental data using these two fitting equations. This precision is determined by analyzing several CW-IRSL curves measured using the same feldspar aliquot.
(c) To demonstrate the mathematical similarities between these two approaches, by examining the corresponding differential equations which involve time dependent recombination probabilities $k(t)$.
(d) To show the robustness of the fitting equations, by examining the dependence of the fitting parameters on the number of data points used during analysis of the CW-IRSL curves.

2. Recombination rate in the model of Jain et al. [22]

In this section we summarize the main physical assumptions and equations used in the model of Jain et al. [22], and discuss the analytical equation used in this paper to fit experimental CW-IRSL curves. The new mathematical result presented in this section is the derivation of the time dependent recombination probabilities $k(t)$ in the semi-analytical model by Jain et al. [22].

The main physical assumption in the model of Jain et al. [22] is the presence of a random distribution of hole traps in the luminescent volume, and an associated range of random nearest-neighbor recombination probabilities. Within the model, stimulated recombination takes place only via the excited state of the electron trap, by either optical or thermal stimulation. The concentration of holes is assumed to be much larger than the concentration of electron traps, and an electron can tunnel only to its nearest hole. In the exact form of the model, one writes a system of differential equations describing the traffic of electrons between the ground state, the excited state and the recombination center. These coupled differential equations contain two variables, namely the distance r' between donor–acceptor pairs and the time, t.

Jain et al. [22] developed also an approximate semi-analytical model to describe the behavior of the system. This second version of the model evolves only in time, and the approximation used is based on introducing a critical tunneling lifetime, τ_c. The equations in the approximate semi-analytical version of the model and for the case of CW-IRSL experiments are as follows [22]:

$$\frac{d\,n_g}{d\,t} = -An_g + Bn_e, \tag{1}$$

$$\frac{d\,n_e}{d\,t} = An_g - Bn_e - \frac{3n_e\rho'^{1/3}}{\tau_c}\left(\ln\frac{n_o}{n}\right)^{2/3} z, \tag{2}$$

$$L(t) = -\frac{d\,m}{d\,t} = \frac{3n_e\rho'^{1/3}}{\tau_c}\left(\ln\frac{n_o}{n}\right)^{2/3} z, \tag{3}$$

$$\tau_c = s^{-1}\exp\left[\left(\frac{1}{\rho'}\ln\frac{n_o}{n}\right)^{1/3}\right]. \tag{4}$$

The following parameters and symbols are used in these expressions: n_g and n_e are the instantaneous concentrations of electrons in the ground state and in the excited state correspondingly. m is the instantaneous concentration of acceptors (holes), n is the instantaneous concentration of all the donors, and N represents the instantaneous concentration of electrons in thermally disconnected states, such that $m = n+N = (n_g+n_e)+N$. The parameter A represents the excitation rate from the ground to the excited state, and is equal to $A = \sigma(\lambda)I$ for the case of optical excitation. Here λ is the optical stimulation wavelength, $\sigma(\lambda)$is the optical absorption cross-section and I is the light intensity ($\mathrm{cm}^{-2}\mathrm{s}^{-1}$). Additional parameters are the dimensionless number density of acceptors ρ', the critical tunneling lifetime τ_c, the thermal excitation frequency factor s, and $z=1.8$, a dimensionless constant introduced in the model. B is the relaxation rate from the excited into the ground state, and $L(t)$ is the instantaneous tunneling luminescence from recombination via the excited state. Under the detailed balance principle one also has $B=s$. Perhaps the most important physical parameters in the model are the constant dimensionless number density of acceptors ρ', and the critical tunneling lifetime τ_c which depends on the instantaneous concentration of donors n as shown in Eq. (4).

Kitis and Pagonis [28] showed that under certain simplifying physical assumptions, the system of Eqs. (1)–(4) can be replaced accurately with the following single differential equation:

$$\frac{d\,n_g}{d\,t} = -\frac{3\rho'^{1/3}Az}{s\tau_c}\left(\ln\frac{n_o}{n}\right)^{2/3} n_g \tag{5}$$

Furthermore, these authors obtained the following analytical solutions for the CW-IRSL luminescence intensity $L(t)$ at time t:

$$L(t) = 3n_o\rho' F(t)^2 zAe^{-F(t)}e^{-\rho'[F(t)]^3}, \tag{6}$$

with the quantity $F(t)$ defined by the following equation:

$$F(t) = \ln(1+z\int_0^t Adt') = \ln(1+zAt). \tag{7}$$

By substituting Eq. (7) into (6), the following analytical equation is obtained:

$$L(t) = \frac{C\left[\ln(1+zAt)\right]^2 e^{-\rho'[\ln(1+zAt)]^3}}{1+zAt}, \tag{8}$$

where C is a constant amplitude which depends on the experimental conditions. Eq. (8) is used to fit the experimental CW-IRSL curves in this paper. The three variable fitting parameters are C, ρ', and A. From a practical point of view, one fits the experimental CW-IRSL curves using Eq. (8), in order to obtain the three fitting parameters C, ρ', and A.

Eq. (8) is plotted as a function of time in Fig. 1a–d for several physically reasonable values of the optical stimulation probability A and of the dimensionless density, ρ'. Fig. 1a shows the

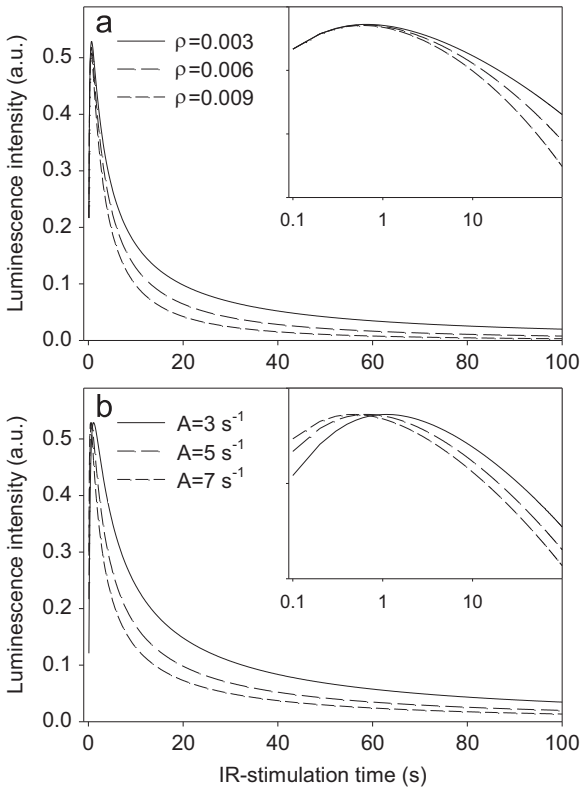

Fig. 1. (a) Simulated dependence of the luminescence intensity using Eq. (8) for several values of the dimensionless density ρ'. (b) Simulations for several values of the optical stimulation probability A. The insets show the same simulated data on a log–log scale.

simulated luminescence intensity $L(t)$ for several values of the dimensionless density, $\rho'=0.003$, 0.006 and 0.009. The inset shows the same data on a log-log scale, in order to show more clearly the differences between the CW-IRSL curves. The simulated curves in Fig. 1a and b show that ρ' does not affect the initial part of the curve for times $t<1$ s, but it does affect strongly the final part of the curve at long IR-stimulation times. As the value of ρ' increases in Fig. 1(b), the slope of the log–log curves at long times, t, becomes larger and the effective power law coefficient increases.

Fig. 1b shows $L(t)$ for several values of the optical stimulation probability $A=3$, 5, 7 s^{-1} while the value of ρ' is kept constant at $\rho'=0.003$. The inset shows the same data on a log-log scale. The simulated curves in Fig. 1b show that the value of A affects strongly the initial part of the curve for times $t<1$ s, but it has a rather small effect on the slope of the final part of the curve at long IR-stimulation times.

The overall modeled results in Fig. 1 are in agreement with the previous interpretation of the shape of the CW-IRSL curves in which initially only nearby electron–hole pairs recombine rather quickly, and therefore the initial CW-IRSL curve decreases rapidly (Thomsen et al. [24,25]). At later IR-stimulation times only far away pairs recombine at a much slower rate, and the CW-IRSL curve decreases at a much slower rate, yielding the well-known power law of luminescence.

We now derive an analytical expression for the effective recombination probability $k_{eff}(t)$ within the model of Jain et al. [22].

The explicit solution for Eq. (5) was given in Kitis and Pagonis [28], their Eq. (17):

$$n_g(t)=n_o e^{-\rho'\left[\ln(1+zAt)\right]^3}. \tag{9}$$

By substituting Eq. (9) into Eq. (4), one obtains the following expression for the critical lifetime, τ_c:

$$\tau_c=s^{-1}\exp\left(\frac{r_c'}{(\rho')^{1/3}}\right)=s^{-1}\exp\left(\frac{(\rho')^{1/3}ln(1+zAt)}{(\rho')^{1/3}}\right)=s^{-1}(1+zAt). \tag{10}$$

Hence within the semi-analytical model of Jain et al. [22], the critical lifetime τ_c increases linearly with the IR-stimulation time t. This was also discussed previously in some detail by Huntley [16] and Jain et al. [22]. By substituting Eq. (9) into the single differential Eq. (5) and after some straightforward algebra one obtains:

$$\frac{d\,n_g}{d\,t}=-\frac{3\rho'^{1/3}Az}{s\tau_c}\left[(\rho')^{1/3}\ln(s\tau_c)\right]^2 n_g=-\frac{3\rho' Az\left[\ln(s\tau_c)\right]^2}{s\tau_c}n_g=-k_{eff}(t)n_g, \tag{11}$$

where the time-dependent quantity $k_{eff}(t)$ represents an effective time-dependent recombination probability for the IRSL process (in s^{-1}), and is defined here as follows:

$$k_{eff}(t)=\frac{3\rho' Az\left[\ln(s\tau_c)\right]^2}{s\tau_c}. \tag{12}$$

By substituting Eq. (10) into Eq. (12), the effective decay rate $k_{eff}(t)$ becomes:

$$k_{eff}(t)=\frac{3\rho' Az\left[\ln(1+zAt)\right]^2}{1+zAt}. \tag{13}$$

For typical values of A and for most practical situations one has $zAt\gg1$, so Eq. (13) simplifies to:

$$k_{eff}(t)=\frac{3\rho'\left[\ln(1+zAt)\right]^2}{t}. \tag{14}$$

This equation indicates that as the IR-stimulation time t increases, the recombination probability $K_{eff}(t)$ for the CW-IRSL process decreases monotonically and approaches an approximate $1/t$ power law at large stimulation times

In the next section the corresponding time dependent recombination probability $k_B(t)$ for the Becquerel decay law is discussed in some detail, and are compared with the results from Eq. (14).

3. Recombination rate in the Becquerel decay law

The mathematical form of the Becquerel decay law is (Berberan-Santos et al. [27]):

$$L(t)=\frac{n_o}{\left[1+(1-\beta)(t/\tau_o)\right]^{1/(1-\beta)}} \tag{15}$$

In general the control parameter β ranges from 0 to 1 and depends on the lattice fractal dimension and luminescence mechanism, while τ_o is a characteristic time parameter for the luminescence process. The constant n_o represents the luminescence intensity at time $t=0$. The Becquerel law is obtained as the solution $L(t)=d\,N/d\,t$ of the differential equation

$$\frac{d\,N}{d\,t}=-k_B(t)N=-\frac{1}{\tau(t)}N \tag{16}$$

where $L(t)$ is the luminescence intensity, N in the model represents the total number of electron–hole pairs at time t, and $k_B(t)$ is assumed to be a time-dependent rate constant given by the following equation [27]:

$$k_B(t)=\frac{1}{\tau_o+(1-\beta)t} \tag{17}$$

The differential Eqs. (11) and (16) have the exact same mathematical form, with the corresponding time-dependent recombination probabilities $k_{eff}(t)$ and $k_B(t)$ given by Eqs. (13) and (17).

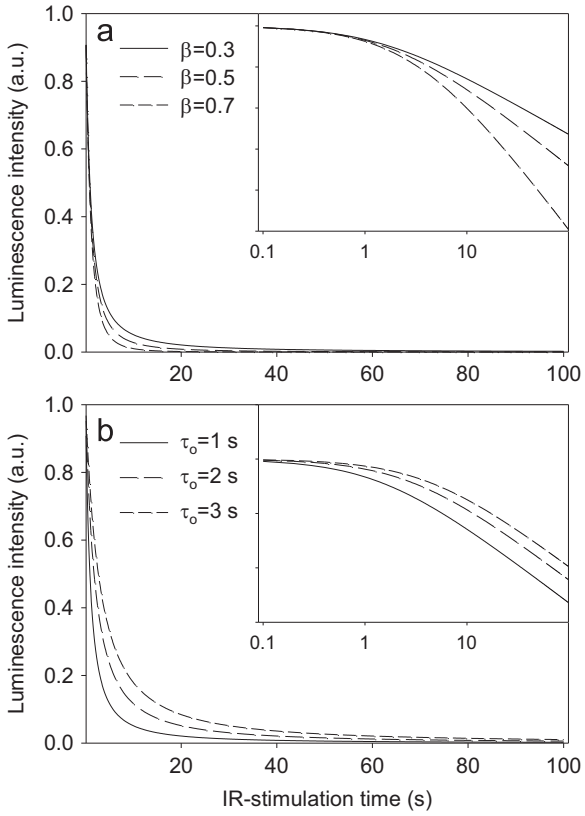

Fig. 2. Simulated dependence of the luminescence intensity $L(t)$using the Becquerel decay law Eq. (15). (a) $L(t)$for several numerical values of the constant β and (b) $L(t)$for several values of the characteristic time τ_o. The insets show the same simulated data on a log–log scale.

From a practical point of view, one can fit the experimental CW-IRSL curves using the Becquerel decay law Eq. (15), in order to obtain the three fitting parameters n_o, τ_o, β. Once the parameters τ_o, β are known, the effective decay constant $k_B(t)$ can be calculated using Eq. (17). Eq. (15) is plotted as a function of time in Fig. 2 for several physically reasonable values of the constant τ_o, β.

Fig. 2a shows the simulated luminescence intensity $L(t)$ for several values of the constant β=0.3, 0.5 and 0.7 while the inset shows the same data on a log–log scale. The simulated curves in Fig. 2a show that β does not affect the initial part of the curve for times $t<1$ s, but it does affect strongly the final part of the curve at long IR-stimulation times. Thus the influence of the parameter β in the Becquerel equation is similar to the effect of the parameter ρ' in Eq. (8). As the value of β increases, the slope of the log–log curves at long stimulation times becomes steeper and the power law coefficient increases.

Fig. 2b shows $L(t)$for several values of the characteristic time $\tau_o=1$, 2, 3 s while the value of β is kept constant at β=0.5, while the inset shows the same data on a log-log scale. The simulated curves in Fig. 2b show that the value of τ_o affects the initial part of the curve for times $t<1$ s, but it has a rather small effect on the slope of the final part of the curve at long IR-stimulation times. Thus the influence of the parameter τ_o in the Becquerel equation is similar to the effect of the optical stimulation parameter A in Eq. (8).

One can also obtain a physical interpretation for the constants τ_o, β in the Becquerel law by considering the effective lifetime $\tau_B(t)=1/k_B(t)$ for the luminescence process, defined as follows:

$$\tau_B(t)=1/k_B(t)=\tau_o+(1-\beta)t \tag{18}$$

According to this equation, the constant $(1-\beta)$ represents physically the rate of decrease of the effective lifetime $\tau_B(t)$ with stimulation time, while the constant $\tau_o$represents the initial rate of decay of the Becquerel decay law.

In the next section the analytical Eqs. (8) and (15) are used to fit experimental data, and the precision and accuracy of these fitting functions are examined in some detail.

4. Results of fitting experimental CW-IRSL curves

4.1. Experimental details

A museum specimen of feldspar (FL3) in the plagioclase series was used in this study. Details about the sample properties, sample preparation and about the experimental setup are given in Morthekai et al. [31]. The IR bleaching was achieved by IR LEDs (870 ± 40 nm) and the luminescence emission was detected using a photomultiplier tube and combination of optical filters transmitting photons in the wavelength region 395 ± 50 nm. The experimental procedure used in this paper is described in a separate experimental study of the effect of a thermal cleaning process on the TL glow curves for this sample (Pagonis et al. [34]). Specifically the TL glow curves are obtained using a $T_{max}-T_{stop}$ thermal cleaning procedure, as follows. A single aliquot of the material is irradiated with a beta dose of 21.3 Gy and then heated up to a temperature T_{stop}. The sample is then exposed to infrared light for 100 s at 50 °C in order to measure the CW-IRSL curve, and then heated all the way to a high temperature of 450 °C to measure the remaining TL glow curve. The process is then repeated several times by irradiating the same aliquot with the same dose and heating to a slightly higher temperature T_{stop} each time, in steps of 10 °C for the complete interval T_{stop}=50–380 °C. This procedure produces a series of TL glow curves which were analyzed in Pagonis et al. [34], as well as a series of CW-IRSL curves which are the subject of the study in this paper.

4.2. Results from fitting experimental data

Fig. 3a shows the result of fitting a typical CW-IRSL curve from sample FL3 (measured at 50 °C) using Eq. (8). The inset shows the same fitted data on a log-log scale. The best fitting values of the three fitting parameters are $C=5.1\times10^5\pm1077$ (counts/0.5 s), $\rho'=0.0115\pm0.0001$ and $A=9.49\pm0.08$ (s^{-1}). The residuals of the un-weighted fitting procedure representing the difference between the experimental data and the corresponding best fit values are shown below the fitted graph. These fitting residuals are seen to be smaller than ~0.4% of the corresponding CW-IRSL intensity for all points along the CW-IRSL signal. Fig. 3b shows the distribution of the residuals fitted to a Gaussian function centered at zero. These residuals are not completely random and do seem to follow a trend at low stimulation times. However, even in the presence of this trend, the residuals show a reasonably good fit to a Gaussian distribution. The quality of the fit to the experimental data can be expressed in a quantitative manner using the well-known figure of merit (FOM). The value of FOM for the fit in Fig. 3 is ~3.5%, indicating a satisfactory fit.

Fig. 4 shows the results of analyzing N=22 experimental CW-IRSL curves similar to the one shown in Fig. 3. These curves were obtained using the experimental procedure described in the previous section, using a single aliquot of sample FL3. Fig. 4a shows the results for the dimensionless density with an average value of $\rho'=0.0119\pm0.0008$ (1σ), while Fig. 4b shows the corresponding histogram for the optical excitation probability $A=9.0\pm0.6$ (s^{-1}). These results indicate that the precision of both extracted fitting parameters ($\rho'$and A) is of the order of ~7%.

Fig. 5 shows the same experimental data as in Fig. 3, but fitted using the Becquerel decay law Eq. (15). The best fitting values of

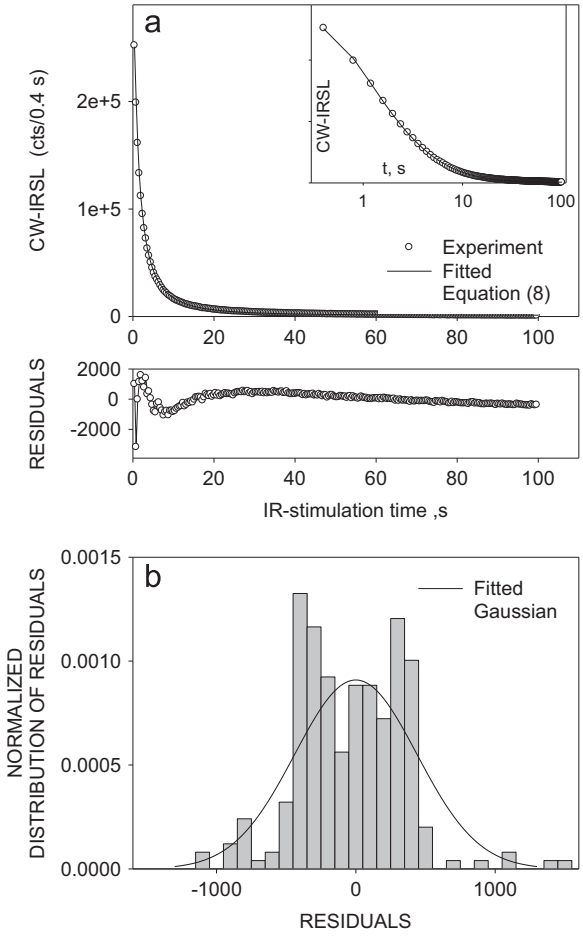

Fig. 3. (a) Typical example of experimental CW-IRSL curve FL3 sample, fitted with the analytical Eq. (8). The fitting residuals are shown underneath the curve. (b) Distribution of the fitting residuals, showing they approximate white noise.

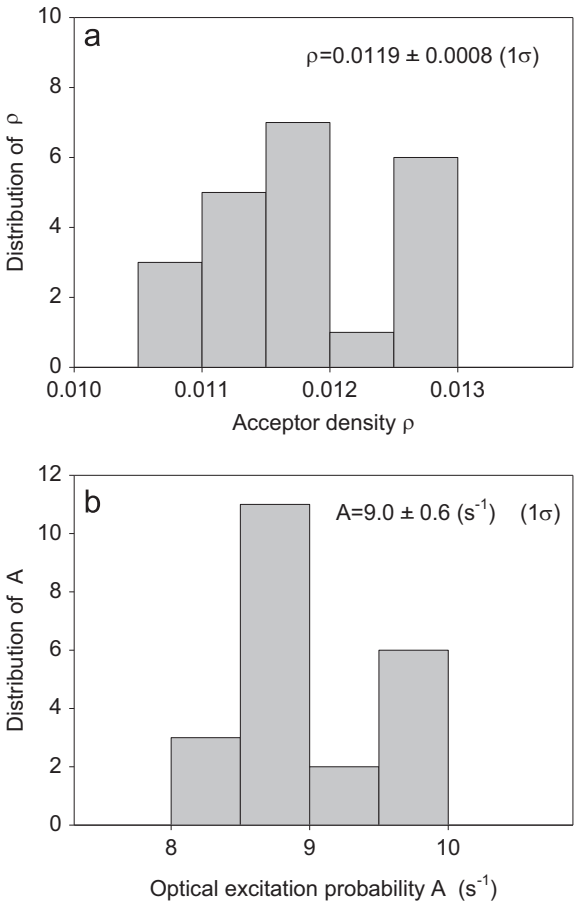

Fig. 4. The results of analyzing $N=22$ experimental CW-IRSL curves similar to the one shown in Fig. 3. The histogram for the dimensionless density ρ' and the corresponding histogram for the optical excitation probability A.

the three fitting parameters are $n_o = 3.3 \times 10^5 \pm 545$ (counts/0.5 s), $\beta = 0.470 \pm 0.001$ and $\tau_o = 1.342 \pm 0.005$ (s). The residuals of the fitting procedure are shown below the fitted graph, and are seen to be better than ~0.3% of the corresponding CW-IRSL intensity for all points along the CW-IRSL signal. The value of FOM for the fit in Fig. 5 is ~2.5%, indicating a satisfactory fit. Fig. 5b shows the distribution of the residuals fitted to a Gaussian function centered at zero. Comparison of the best fits in Figs. 3 and 5 shows that the Becquerel function provides a slightly better fit of the experimental CW-IRSL data than Eq. (8); however, the quality of fit from both fitting equations is excellent.

Fig. 6 shows the results of analyzing the same $N=22$ curves as in Fig. 4, but using the Becquerel decay law. Fig. 6a shows the results for the dimensionless coefficient β with an average value of $\beta = 0.51 \pm 0.03$ (1σ), while Fig. 6b shows the corresponding histogram for the characteristic time $\tau_o = 1.5 \pm 0.1$ (s). These results indicate that the precision of both extracted fitting parameters (β and τ_o) is of the order of ~6–7%.

4.3. Comparison of the recombination probabilities in the two approaches

Once the values of the parameters ρ' and A are known from the best fit using Eq. (8), the effective recombination probability k_{eff} can be calculated using expression (13) as a function of the IR-stimulation time, t. The result is shown in Fig. 7 in which the k_{eff} values decrease from an initial value of ~0.53 s^{-1} at time $t=0$ to a value of ~0.02 s^{-1} at the end of CW-IRSL curve.

Similarly once the values of the parameters τ_o, β are known from the best fit obtained using Eq. (15), the recombination probability $k_B(t)$ can be calculated using expression (17) as a function of the IR-stimulation time, t. The result is also shown in Fig. 7, indicating that the numerical values and time variations of the recombination probabilities $k_{eff}(t)$ and $k_B(t)$ are very similar in this numerical example. This explains the success of both mathematical descriptions in describing accurately the shape of the CW-IRSL curves.

Some differences between the values of $k_{eff}(t)$ and $k_B(t)$ are seen at large times in Fig. 7. However, overall there is rather remarkable numerical similarity between the two mathematical approaches. This similarity explains the very good fits obtained using either Eq. (8) derived by Kitis and Pagonis [28], or the Becquerel law Eq. (15).

One can also demonstrate the similarities between the two types of fits by using the Becquerel equation to create a curve with known parameters, and subsequently fitting this curve with Eq. (8). When such a procedure was undertaken, it was found that the fitted function represented very well the Becquerel curve, with a FOM value 1–5% for this fitting procedure. A similar good representation was achieved when using the reverse fitting procedure, i.e. when fitting a curve generated using Eq. (8) with the Becquerel function.

4.4. Effect of the number of experimental points used in the fitting process

Fig. 8 shows the effect of varying the number of points used during the fitting procedure, and how this affects the robustness of the extracted parameters in the two mathematical approaches.

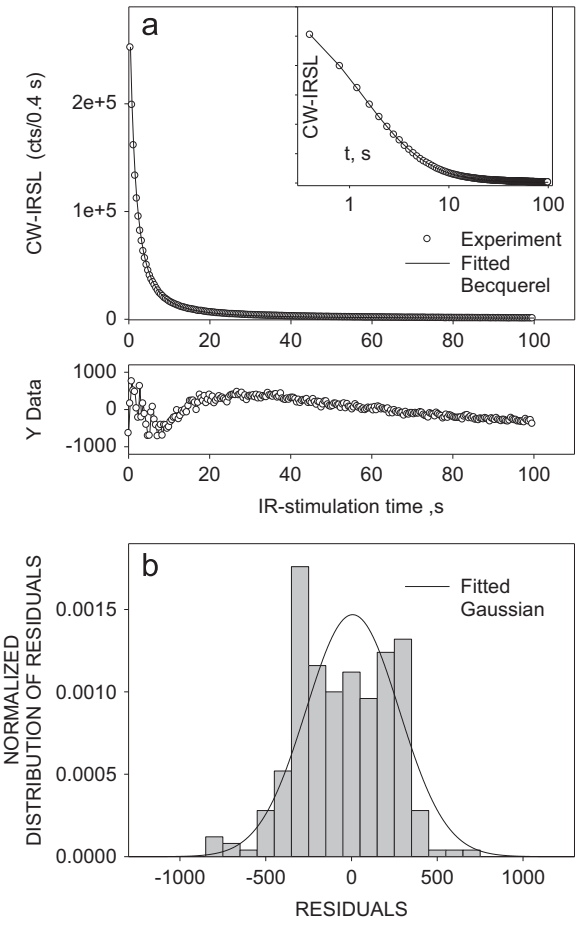

Fig. 5. Example of fit to same data as in Fig. 2, using the Becquerel decay law Eq. (17). The fitting residuals are shown underneath the curve The distribution of the fitting residuals.

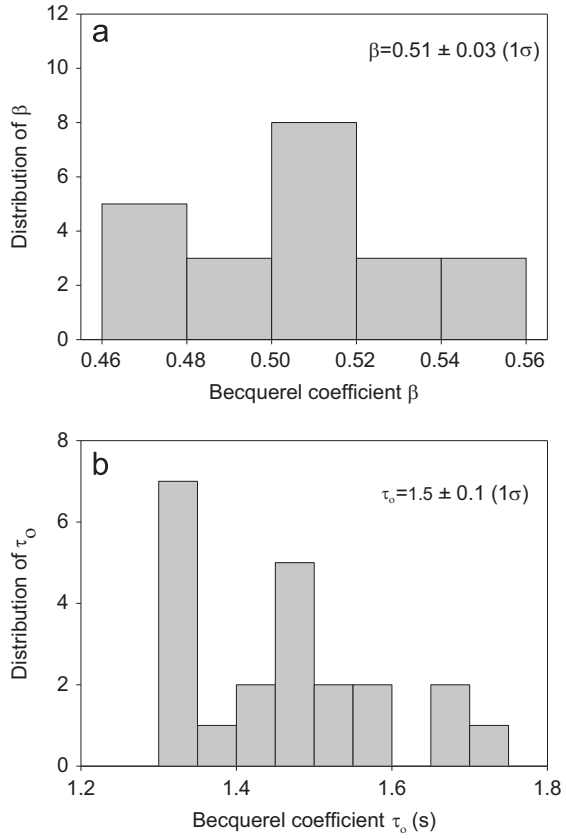

Fig. 6. Histograms of the fitting parameters for $N=22$ IRSL curves from the same aliquot using the Becquerel decay law.

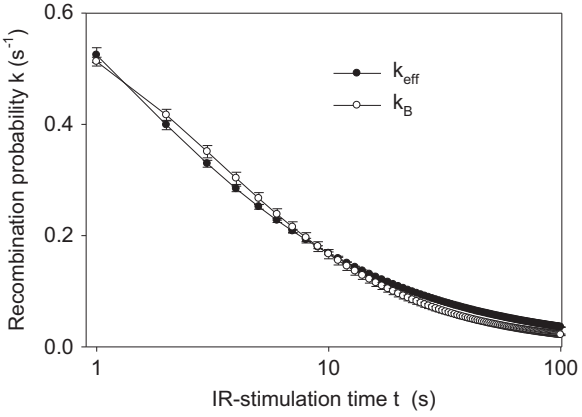

Fig. 7. Comparison of the effective recombination probabilities k_{eff} calculated using expression (13) and k_B calculated using expression (17), as a function of the IR-stimulation time, t. The numerical values of the recombination probabilities are seen to be almost identical in this example.

The experimental points in the CW-IRSL curves studied in this paper extend up to a total IR-stimulation time of 100 s and were measured every 0.5 s, and therefore contain a total of $N=200$ experimental points. Fig. 8a shows the dependence of the fitting parameters ρ' and A on the IR-stimulation time, and therefore on the number of points used in the fitting procedure. The values of ρ' and A are almost constant, even when using only the first 25 s (or first 50 experimental points) of the CW-IRSL signal in the fitting procedure. This indicates that the extracted parameters are likely to be independent of each other and of the number of points, N, used in the fitting procedure, and to represent the correct values near a universal minimum of the fitting process.

Fig. 8b shows the corresponding results for the Becquerel parametersβ and τ_o, which are very similar to the results of Fig. 8a. Once more, the extracted fitted parameters do not depend on the number of points, N, used during the fitting procedure, at least for $N>50$.

5. Discussion and conclusions

This paper showed that both the Kitis–Pagonis Eq. (8) and the compressed hyperbola Eq. (15) can be used to describe mathematically experimental CW-IRSL curves in feldspars. Despite its simplicity, the Becquerel decay law produces a slightly better fitting curve around the initial time than Eq. (8) which is based on the model by Jain et al. [22].

Overall, several recent experimental and modeling papers have contributed to a better understanding of the luminescence and tunneling processes in feldspars provided valuable information on the origin of IRSL signals from feldspars, and supported the existence of tunneling processes involving localized recombinations with tunneling taking place from the excited state of the trap, as well as charge migration through the conduction band-tail states (Poolton et al. [18], Jain and Ankjærgaard [19], Ankjærgaard et al. [20], Thomsen et al. [24], Pagonis et al. [29], Kars et al. [30], Morthekai et al. [31]).

The model of Jain et al. [22] has also been used in several recent papers to analyze other types of experimental luminescence data

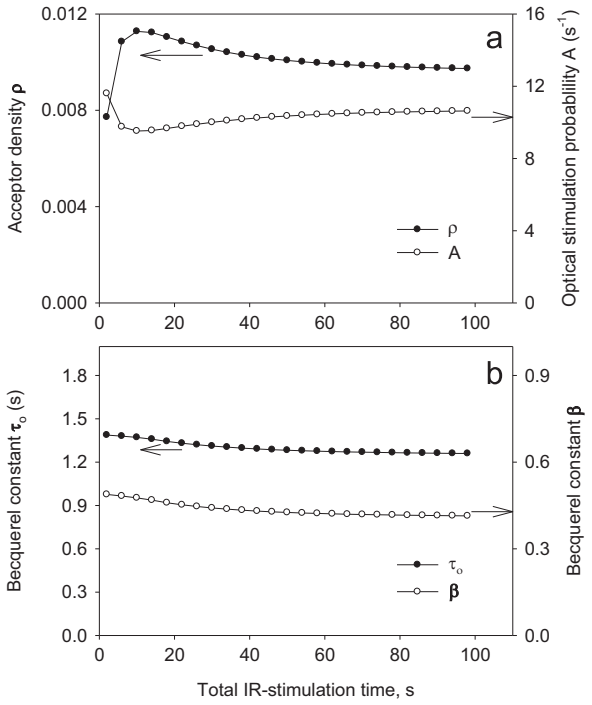

Fig. 8. Study of the effect of the number of points used during the fitting procedure showing that the values of the extracted fitting parameters do not depend on the number of points, *N*. (a) Analysis using the Becquerel equation and (b) Analysis using the KP equation.

from feldspars. Sfamba et al. [32] analyzed isothermal luminescence signals from Durango apatite, and found that these signals could be fitted very accurately with the model of Jain et al. [22]. Also Pagonis et al. [33] analyzed experimental CW-IRSL curves from 24 different types of feldspars by using the analytical Eq. (8) presented in this paper. These authors compared results from natural samples, freshly irradiated samples, samples which had undergone anomalous fading, and K and Na rich extracts. The results of this analysis establish broad numerical ranges for the ρ' used in the model by Jain et al. [22]. Furthermore, all samples exhibited the Becquerel power law of decay with the range of the power law coefficient $\beta = 0.6 \sim 1.1$. In another recent experimental study Pagonis et al. [34] analyzed TL glow curves from feldspar using the model of Jain et al. [22], as well as using the general order kinetics model of TL.

Finally it is noted that in case the fitting of CW-IRSL data with a single component fails, one could use the sum of two or three Becquerel functions to represent the experimental data [35].

Acknowledgements

Experimental work was financially supported by the Department of Science and Technology, India (SR/FTP/ES-56/2011).

References

[1] L. Bøtter-Jensen, S.W.S. McKeever, A.G. Wintle., Optically Stimulated Luminescence Dosimetry, Elsevier, Amsterdam, 2003.
[2] R. Chen, S.W.S. McKeever, Theory of Thermoluminescence and Related Phenomena, World Scientific, Singapore, 1997.
[3] R. Chen, V. Pagonis, Thermally and Optically Stimulated Luminescence: A Simulation Approach, Wiley and Sons, Chichester, 2011.
[4] R. Visocekas, Nucl. Tracks Radiat. Meas. 10 (1985) 521.
[5] R. Visocekas, N.A. Spooner, A. Zink, P. Blank, Radiat. Meas. 23 (1994) 371.
[6] I.K. Bailiff, S.M. Barnett, Radiat. Meas. 23 (1994) 541.
[7] G.A.T. Duller, L. Bøtter-Jensen, Radiat. Prot. Dosim. 47 (1993) 683.
[8] I.K. Bailiff, N.R.J. Poolton, Nucl. Tracks Radiat. Meas. 18 (1991) 111.
[9] N.R.J. Poolton, K.B. Ozanyan, J. Wallinga, A.S. Murray, L. Bøtter-Jensen, Phys. Chem. Minerals 29 (2002) 217.
[10] B. Li, S.-H. Li, Radiat. Meas. 46 (2010) 29.
[11] B. Li, S.-H. Li, J. Phys. D: Appl. Phys. 41 (2008) 225502.
[12] R.H. Kars, J. Wallinga, K.M. Cohen, Radiat. Meas. 43 (2008) 786.
[13] A. Larsen, S. Greilich, M. Jain, A.S. Murray, Radiat. Meas. 44 (2009) 467.
[14] D.J. Huntley, M. Lamothe, Can. J. Earth Sci. 38 (2001) 1093.
[15] C.J. Delbecq, Y. Toyozawa, P.H. Yuster, Phys. Rev. B 9 (1974) 4497.
[16] D.J. Huntley, J. Phys.: Condens. Matter 18 (2006) 1359.
[17] M.R. Baril, 2002. Ph.D. thesis. Simon Fraser University, Burnaby, BC, Canada. Available from: www.cfht.hawaii.edu/~baril/Temp/baril_phdthesis.pdf.
[18] N.R.J. Poolton, R.H. Kars, J. Wallinga, A.J. Bos, J. Phys.: Condens. Matter 21 (2009) 485505.
[19] M. Jain, C. Ankjærgaard, Radiat. Meas. 46 (2011) 292.
[20] C. Ankjærgaard, M. Jain, R. Kalchgruber, T. Lapp, D. Klein, S.W.S. McKeever, A. S. Murray, P. Morthekai, Radiat. Meas. 44 (2009) 576.
[21] V. Pagonis, M. Jain, A.S. Murray, C. Ankjærgaard, R. Chen, Radiat. Meas. 47 (2012) 870.
[22] M. Jain, B. Guralnik, M.T. Andersen, J. Phys.: Condens. Matter 24 (2012) 385402.
[23] A. Molodkov., I. Jaek, V. Vasilchenko, Geochronometria 26 (2007) 11.
[24] K.J. Thomsen, A.S. Murray, M. Jain, L. Bøtter-Jensen, Radiat. Meas. 43 (2008) 1474.
[25] K.J. Thomsen, A.S. Murray, M. Jain, Geochronometria 38 (2011) 1.
[26] M.N. Berberan-Santos (Ed.), Polymers and Nanosystems, Springer, Berlin, 2008.
[27] M.N. Berberan-Santos, E.N. Bodunov, B. Valeur, Chem. Phys. 317 (2005) 57.
[28] G. Kitis, G, V. Pagonis, J. Lumin. 137 (2013) 109.
[29] V. Pagonis, H. Phan, D. Ruth, G. Kitis, Radiat. Meas. 58 (2013) 66.
[30] R.H. Kars, N.R.J. Poolton, M. Jain, C. Ankjærgaard, P. Dorenbos, J. Wallinga, Radiat. Meas. 59 (2013) 103.
[31] P. Morthekai, J. Thomas, M.S. Pandian, V. Balaram, A.K. Singhvi, Radiat. Meas. 47 (2012) 857.
[32] I. Sfamba, G.S. Polymeris, N.C. Tsirliganis, V. Pagonis, G. Kitis, Nucl. Inst. Methods Phys. Res. B 320 (2014) 57.
[33] V. Pagonis, M. Jain, K.J. Thomsen, A.S. Murray, J. Lumin. 153 (2014) 96–103.
[34] V. Pagonis, P. Morthekai, G. Kitis, Geochronometria 41 (2014) 168.
[35] F. Menezes, A. Fedorov, C. Baleizão, B. Valeur, M.N. Berberan-Santos, Methods Appl. Fluoresc. 1 (2013) 015002.